Observation of nuclear scaling in the $A(e,e')$ reaction at $x_B>1$

K. Sh. Egiyan,[1] N. Dashyan,[1] M. Sargsian,[11] S. Stepanyan,[36,27] L. B. Weinstein,[27] G. Adams,[31] P. Ambrozewicz,[11] E. Anciant,[6] M. Anghinolfi,[16] B. Asavapibhop,[23] G. Asryan,[1] G. Audit,[6] T. Auger,[6] H. Avakian,[36] H. Bagdasaryan,[27] J. P. Ball,[2] S. Barrow,[12] M. Battaglieri,[16] K. Beard,[20] I. Bedlinski,[19] M. Bektasoglu,[26,21] M. Bellis,[31] N. Benmouna,[13] N. Bianchi,[15] A. S. Biselli,[4] S. Boiarinov,[19] B. E. Bonner,[32] S. Bouchigny,[17] R. Bradford,[4] D. Branford,[10] W. J. Briscoe,[13] W. K. Brooks,[36] V. D. Burkert,[36] C. Butuceanu,[40] J. R. Calarco,[24] D. S. Carman,[4] B. Carnahan,[5] C. Cetina,[13] L. Ciciani,[27] P. L. Cole,[35] A. Coleman,[40] D. Cords,[36] J. Connelly,[13] P. Corvisiero,[16] D. Crabb,[39] H. Crannell,[5] J. P. Cummings,[31] E. DeSanctis,[15] R. DeVita,[16] P. V. Degtyarenko,[36] R. Demirchyan,[1] H. Denizli,[29] L. Dennis,[12] K. V. Dharmawardane,[27] K. S. Dhuga,[13] C. Djalali,[34] G. E. Dodge,[27] D. Doughty,[7,36] P. Dragovitsch,[12] M. Dugger,[2] S. Dytman,[29] O. P. Dzyubak,[34] M. Eckhause,[40] H. Egiyan,[36] L. Elouadrhiri,[36] A. Empl,[31] P. Eugenio,[12] R. Fatemi,[39] R. J. Feuerbach,[4] J. Ficenec,[38] T. A. Forest,[27] H. Funsten,[40] M. Gai,[8] G. Gavalian,[24] S. Gilad,[22] G. P. Gilfoyle,[33] K. L. Giovanetti,[20] P. Girard,[34] C. I. O. Gordon,[14] K. Griffioen,[40] M. Guidal,[17] M. Guillo,[34] L. Guo,[36] V. Gyurjyan,[36] C. Hadjidakis,[17] R. S. Hakobyan,[5] J. Hardie,[7,36] D. Heddle,[7,36] P. Heimberg,[13] F. W. Hersman,[24] K. Hicks,[26] R. S. Hicks,[23] M. Holtrop,[24] J. Hu,[31] C. E. Hyde-Wright,[27] Y. Ilieva,[13] M. M. Ito,[36] D. Jenkins,[38] K. Joo,[36] J. H. Kelley,[9] M. Khandaker,[25] D. H. Kim,[21] K. Y. Kim,[29] K. Kim,[21] M. S. Kim,[21] W. Kim,[21] A. Klein,[27] F. J. Klein,[36,5] A. Klimenko,[27] M. Klusman,[31] M. Kossov,[19] L. H. Kramer,[11,36] Y. Kuang,[40] S. E. Kuhn,[27] J. Kuhn,[4] J. Lachniet,[4] J. M. Laget,[6] D. Lawrence,[23] Ji Li,[31] K. Lukashin,[36,5] J. J. Manak,[36] C. Marchand,[6] L. C. Maximon,[13] S. McAleer,[12] J. McCarthy,[39] J. W. C. McNabb,[4] B. A. Mecking,[36] S. Mehrabyan,[29] J. J. Melone,[14] M. D. Mestayer,[36] C. A. Meyer,[4] K. Mikhailov,[19] R. Minehart,[39] M. Mirazita,[15] R. Miskimen,[23] L. Morand,[6] S. A. Morrow,[6] M. U. Mozer,[26] V. Muccifora,[15] J. Mueller,[29] L. Y. Murphy,[13] G. S. Mutchler,[32] J. Napolitano,[31] R. Nasseripour,[11] S. O. Nelson,[9] S. Niccolai,[13] G. Niculescu,[26] I. Niculescu,[20,13] B. B. Niczyporuk,[36] R. A. Niyazov,[27] M. Nozar,[36] G. V. O'Rielly,[13] A. K. Opper,[26] M. Osipenko,[16] K. Park,[21] E. Pasyuk,[2] G. Peterson,[23] S. A. Philips,[13] N. Pivnyuk,[19] D. Pocanic,[39] O. Pogorelko,[19] E. Polli,[15] S. Pozdniakov,[19] B. M. Preedom,[34] J. W. Price,[3] Y. Prok,[39] D. Protopopescu,[14] L. M. Qin,[27] B. A. Raue,[11,36] G. Riccardi,[12] G. Ricco,[16] M. Ripani,[16] B. G. Ritchie,[2] F. Ronchetti,[15,30] P. Rossi,[15] D. Rowntree,[22] P. D. Rubin,[33] F. Sabatié,[6,27] K. Sabourov,[9] C. Salgado,[25] J. P. Santoro,[38,36] V. Sapunenko,[16] R. A. Schumacher,[4] V. S. Serov,[19] Y. G. Sharabian,[1,36] J. Shaw,[23] S. Simionatto,[13] A. V. Skabelin,[22] E. S. Smith,[36] L. C. Smith,[39] D. I. Sober,[5] M. Spraker,[9] A. Stavinsky,[19] P. Stoler,[31] I. Strakovsky,[13] S. Strauch,[13] M. Strikman,[28] M. Taiuti,[16] S. Taylor,[32] D. J. Tedeschi,[34] U. Thoma,[36,18] R. Thompson,[29] L. Todor,[4] C. Tur,[34] M. Ungaro,[31] M. F. Vineyard,[37] A. V. Vlassov,[19] K. Wang,[39] A. Weisberg,[26] H. Weller,[9] D. P. Weygand,[36] C. S. Whisnant,[34,20] E. Wolin,[36] M. H. Wood,[34] A. Yegneswaran,[36] J. Yun,[27] B. Zhang,[22] J. Zhao,[22] and Z. Zhou[22,7]

(CLAS Collaboration)

[1]*Yerevan Physics Institute, Yerevan 375036, Armenia*
[2]*Arizona State University, Tempe, Arizona 85287-1504, USA*
[3]*University of California at Los Angeles, Los Angeles, California 90095-1547, USA*
[4]*Carnegie Mellon University, Pittsburgh, Pennsylvania 15213, USA*
[5]*Catholic University of America, Washington, D.C. 20064, USA*
[6]*CEA-Saclay, Service de Physique Nucléaire, F91191 Gif-sur-Yvette, Cedex, France*
[7]*Christopher Newport University, Newport News, Virginia 23606, USA*
[8]*University of Connecticut, Storrs, Connecticut 06269, USA*
[9]*Duke University, Durham, North Carolina 27708-0305, USA*
[10]*Edinburgh University, Edinburgh EH9 3JZ, United Kingdom*
[11]*Florida International University, Miami, Florida 33199, USA*
[12]*Florida State University, Tallahassee, Florida 32306, USA*
[13]*The George Washington University, Washington, D.C. 20052, USA*
[14]*University of Glasgow, Glasgow G12 8QQ, United Kingdom*
[15]*INFN, Laboratori Nazionali di Frascati, Frascati, Italy*
[16]*INFN, Sezione di Genova, I-16146 Genova, Italy*
[17]*Institut de Physique Nucleaire ORSAY, Orsay, France*
[18]*Institute für Strahlen und Kernphysik, Universität Bonn, Bonn, Germany*
[19]*Institute of Theoretical and Experimental Physics, Moscow 117259, Russia*
[20]*James Madison University, Harrisonburg, Virginia 22807, USA*
[21]*Kungpook National University, Taegu 702-701, South Korea*
[22]*Massachusetts Institute of Technology, Cambridge, Massachusetts 02139-4307, USA*
[23]*University of Massachusetts, Amherst, Massachusetts 01003, USA*
[24]*University of New Hampshire, Durham, New Hampshire 03824-3568, USA*
[25]*Norfolk State University, Norfolk, Virginia 23504, USA*
[26]*Ohio University, Athens, Ohio 45701, USA*
[27]*Old Dominion University, Norfolk, Virginia 23529, USA*

 ©2003 The American Physical Society

[28]*Pennsylvania State University, State College, Pennsylvania 16802, USA*
[29]*University of Pittsburgh, Pittsburgh, Pennsylvania 15260, USA*
[30]*Universita' di ROMA III, I-00146 Roma, Italy*
[31]*Rensselaer Polytechnic Institute, Troy, New York 12180-3590, USA*
[32]*Rice University, Houston, Texas 77005-1892, USA*
[33]*University of Richmond, Richmond, Virginia 23173, USA*
[34]*University of South Carolina, Columbia, South Carolina 29208, USA*
[35]*University of Texas at El Paso, El Paso, Texas 79968, USA*
[36]*Thomas Jefferson National Accelerator Facility, Newport News, Virginia 23606, USA*
[37]*Union College, Schenectady, New York 12308, USA*
[38]*Virginia Polytechnic Institute and State University, Blacksburg, Virginia 24061-0435, USA*
[39]*University of Virginia, Charlottesville, Virginia 22901, USA*
[40]*College of William and Mary, Williamsburg, Virginia 23187-8795, USA*
(Received 18 January 2003; published 29 July 2003)

The ratios of inclusive electron scattering cross sections of ^{4}He, ^{12}C, and ^{56}Fe to ^{3}He have been measured for the first time. It is shown that these ratios are independent of x_B at $Q^2>1.4$ GeV^2 for $x_B>1.5$, where the inclusive cross section depends primarily on the high momentum components of the nuclear wave function. The observed scaling shows that the momentum distributions at high-momenta have the same shape for all nuclei and differ only by a scale factor. The observed onset of the scaling at $Q^2>1.4$ GeV^2 and $x_B>1.5$ is consistent with the kinematical expectation that two-nucleon short range correlations (SRC) dominate the nuclear wave function at $p_m \gtrsim 300$ MeV/c. The values of these ratios in the scaling region can be related to the relative probabilities of SRC in nuclei with $A \geqslant 3$. Our data, combined with calculations and other measurements of the ^{3}He/deuterium ratio, demonstrate that for nuclei with $A \geqslant 12$ these probabilities are 4.9–5.9 times larger than in deuterium, while for ^{4}He it is larger by a factor of about 3.8.

DOI: 10.1103/PhysRevC.68.0143XX PACS number(s): 25.10.+s, 25.30.Fj

I. INTRODUCTION

Due to the strong interaction and short distances between the nucleons in nuclei, there is a significant probability for nucleon wave functions to overlap, resulting in short range nucleon-nucleon correlations (SRC) in nuclei [1]. Investigation of SRC is important for at least two reasons. First, because of the short range nature of these correlations, they should contribute significantly to the high-momentum component of the nuclear wave function. Second, scattering from nucleons in SRC will provide unique data on the modification of deeply bound nucleons, which is extremely important for a complete understanding of nucleon structure in general.

High-energy inclusive electron scattering from nuclei, $A(e,e')$, is one of the simplest ways to investigate SRC. In particular, it is probably the best way to measure the probabilities of SRC in nuclei. The main problem in these studies is selecting the electron-SRC scattering events from the orders-of-magnitude larger background of inelastic and/or quasielastic interaction of electrons with the uncorrelated low-momentum nucleons.

By measuring cross sections at

$$x_B=\frac{Q^2}{2M\nu}>1, \tag{1}$$

contributions from inelastic electron-nucleon scattering and meson exchange currents (at high Q^2) can be significantly reduced, which corresponds to studying the low-energy-loss side of the quasielastic peak. In Eq. (1), Q^2 is the four-momentum squared of the virtual photon ($Q^2=-q^\mu q_\mu>0$), ν is the energy transfer, M is the nucleon mass, and x_B is the Bjorken scaling variable.

Many previous analyses of data in this kinematic region concentrate on using y scaling to deconvolute the nuclear wave function from the inclusive cross section (see, e.g., Refs. [2,3]). This deconvolution, while necessary for extracting momentum distributions, significantly increases the systematic uncertainty in the extraction of SRC probabilities. Moreover, since the contribution from the final state interaction is basically unknown, the extraction of the SRC probabilities in the ground state nuclear wave function became more problematic.

Meanwhile, the data at $x_B>1$ can be used to directly measure the probability of finding SRC in nuclei using another technique. There are theoretical predictions that at momenta higher than the Fermi momentum, nucleon momentum distributions in light and heavy nuclei are similar (see, e.g., Ref. [4] in which this result is obtained based on variational calculations of ground state wave function of ^{16}O using realistic $2N$ and $3N$ interactions, as well as Ref. [5] in which a similar result is obtained for ^{3}He and infinite nuclear matter).

This implies that they originate predominantly from the interaction between two nearby nucleons, i.e., due to SRC. If the $A(e,e')$ cross section depends primarily on the nuclear wave function, and the shape of this wave function at high momentum is really universal, then in this high-momentum region the ratio of weighted (e,e') cross sections for differ-

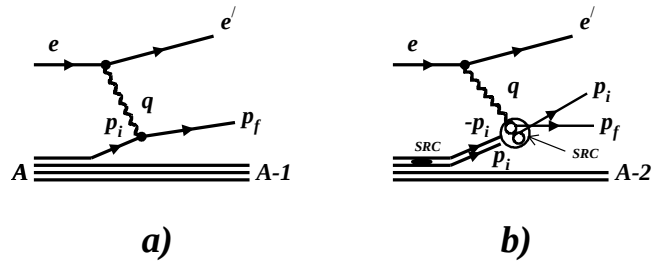

FIG. 1. Two mechanisms of $A(e,e')$ scattering. (a) Single nucleon model; (b) short range correlation model.

ent nuclei[1] should scale, i.e., they should be independent of electron scattering variables (Q^2 and x_B), with the magnitude of the scaling factor being proportional to the relative probability of SRC in the two nuclei [6,7].

In Ref. [7] this was checked by analyzing existing SLAC $A(e,e')$ data for deuterium [8–10] and heavier nuclei [11]. They found an indication of scaling at $Q^2>1$ GeV^2 and $x_B \geqslant 1.5$. However, since the data for deuterium and the heavy nuclei were collected in different experiments at similar Q^2 but at different electron scattering angles and incident electron energies, to find the ratios at the same values of (x_B, Q^2), a complicated fitting and interpolation procedure was applied [7] to the data. The main problem was that the cross sections varied very strongly with angle, incident energy, and Q^2. To simplify the interpolation, the electron-deuteron cross section was first divided by the theoretical calculation within the impulse approximation. Therefore, the data are not purely experimental, since they include the theoretical calculations, and the ratios may have been affected by the fitting and interpolation procedures.

In this work, the yields of the reaction $A(e,e')$ for ^{3}He, ^{4}He, ^{12}C, and ^{56}Fe targets are measured in the same kinematical conditions, and the ratios $A(e,e')/^3\mathrm{He}(e,e')$ are obtained for $1<x_B<2$ and $Q^2>0.65$ GeV^2. Furthermore, using the scaling behavior of these ratios, the relative probability of NN SRC for the various nuclei have been extracted.

II. KINEMATICS AND PREDICTIONS

In order to suppress the background from quasielastic interactions of electrons with the uncorrelated low-momentum nucleons [see Fig. 1(a)], we further restrict the kinematic variables x_B and Q^2.

For quasielastic $A(e,e')$ scattering, x_B, Q^2, and the minimum $A-1$ recoil momentum contributing to the reaction are related by energy and momentum conservation:

$$(q+p_A-p_{A-1})^2=p_f^2=m_N^2, \tag{2}$$

[1]Hereafter, by the ratio of the cross sections we will mean the ratios of the cross sections weighted by A. We will separately discuss effects due to $\sigma_{ep}>\sigma_{en}$ which are important for ^{3}He due to Z not equal to N.

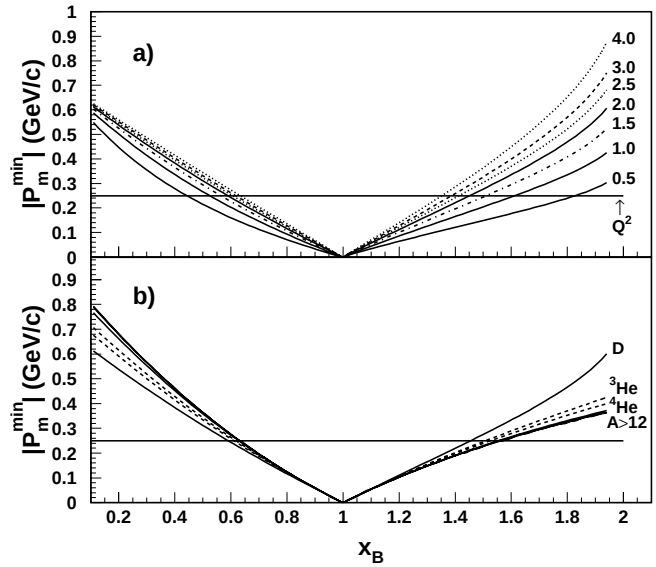

FIG. 2. The minimum recoil momentum as a function of x_B. (a) For deuterium at several Q^2 (in GeV^2); (b) for different nuclei at $Q^2=2.0$ GeV^2. Horizontal lines at 250 MeV/c indicate the Fermi momentum typical of the uncorrelated motion of nucleons in nuclei.

where q, p_A, p_{A-1}, and p_f are the four-momenta of the virtual photon, target nucleus, residual $A-1$ system, and knocked-out nucleon, respectively (note that only q and p_A are known). From Eq. (2), one obtains

$$\Delta M^2-Q^2+\frac{Q^2}{m_N x_B}(M_A-\sqrt{M_{A-1}^2+\vec{p}_m{}^2})-2\vec{q}\cdot\vec{p}_m -2M_A\sqrt{M_{A-1}^2+\vec{p}_m{}^2}=0, \tag{3}$$

where $\Delta M^2=M_A^2+M_{A-1}^2-m_N^2$ and $\vec{p}_m=\vec{p}_f-\vec{q}=-\vec{p}_{A-1}$ is the recoil momentum involved in the reaction (sometimes referred to as the "missing momentum" in $(e,e'p)$ reactions). Equation (3) defines a simple relationship between $|\vec{p}_m{}^{min}|$ and x_B at fixed Q^2. At $x_B>1$, this minimum occurs when the $A-1$ system is in the ground state and $\vec{p}_m \| \vec{q}$. This relation for deuterium at various values of Q^2 is shown in Fig. 2(a). Figure 2(b) shows the same relationship for various nuclei at $Q^2=2$ GeV^2. Note that this relationship is different for the different nuclei, due primarily to differences in the mass of the recoil $A-1$ system. This minimum recoil momentum is one of the possible definitions of the scaling variable y.

One can see from Fig. 2 that for any nucleus A and fixed Q^2, we can find the value x_B^o such that at $x_B > x_B^o$ the magnitude of the minimum recoil momentum, $|\vec{p}_m^{min}|$, contributing to the reaction, exceeds the average Fermi momentum in nucleus A.

It should be pointed out that the initial momentum of the struck nucleon $\vec{p}_i$ is equal to $\vec{p}_m$ only in the simplest model where the virtual photon is absorbed on one nucleon and that nucleon leaves the nucleus without further interactions (the plane wave impulse approximation). In reality, the (e,e')

reaction effectively integrates over many values of $p_m \geqslant p_m^{min}$. In addition, this simple relation between recoil momentum and initial momentum is modified by final state interactions (FSI) and the excitation energy of the residual nucleus. These make it difficult to determine the nuclear wave function directly from (e,e') cross sections. However, for our purposes, it is sufficient to know that when the minimum recoil momentum contributing to the reaction is much larger than the Fermi momentum, the initial momentum of the struck nucleon will also be larger.

Let us now consider various predictions of the ratios of weighted (e,e') cross sections for different nuclei. In the mechanism for inclusive (e,e') scattering at $x_B>1$ with virtual photon absorption on a single nucleon and the $A-1$ system recoiling intact without FSI [see Fig. 1(a)], the minimum recoil momentum for different nuclei at fixed Q^2 differs, and this difference increases with x_B (see Fig. 2). Therefore, the cross section ratio between different nuclei will increase with increasing x_B and will not scale.

In the short range correlation model of Frankfurt and Strikman [1] [see Fig. 1(b)] the high-momentum part of the nuclear momentum distribution is due to correlated nucleon pairs. This means that when the electron scatters from a high-momentum nucleon in the nucleus, we can consider this scattering as an electron-deuterium interaction with the spectator $A-2$ system at rest. (The effect of pair motion is discussed below.) Therefore, according to Fig. 2(a), starting from some threshold x_B^0 for fixed Q^2 the cross section ratio

$$R(A_1,A_2)=\frac{\sigma(A_1,Q^2,x_B)/A_1}{\sigma(A_2,Q^2,x_B)/A_2}, \tag{4}$$

where $\sigma(A_1,Q^2,x_B)$ and $\sigma(A_2,Q^2,x_B)$ are the inclusive electron scattering cross sections from nuclei with atomic numbers A_1 and A_2, respectively, will scale (will be constant). Scaling results from the dominance of SRC in the high-momentum component of the nuclear wave function, and it should be observed, for example, for the cross section ratios of heavy nuclei to light nuclei such as ^{3}He.

Figure 3(a) shows $R(^{12}\mathrm{C},^3\mathrm{He})$ as a function of x_B for Q^2 from 1.5 to 2.5 GeV^2 calculated in the SRC model [12](for details, see also Ref. [13]). The ratio for $A_1=^{56}$Fe and $A_2=^3$He is shown in Fig. 3(b). The calculations used the Faddeev wave function for ^{3}He calculated using the Bonn NN potential [14]. The momentum distributions for heavier nuclei have been modeled through a two component of momentum distribution using mean field distributions for small nucleon momenta and using the deuteron momentum distribution for $p>250$ MeV/c, scaled by factor $a_2(A)$, per-nucleon probability of NN SRC in nucleus A, estimated from Ref. [7]. The mean field momentum distributions used the harmonic oscillator wave function for ^{12}C and the quasiparticle Lagrange method of Ref. [15] for ^{56}Fe. For the description of the eN interaction, the inelastic form factor parametrization of Ref. [16] and the dipole elastic form factors have been used. These calculations are in reasonable agreement with existing $A(e,e')X$ experimental data from the SLAC [17] and from the Jefferson Lab Hall C [19].

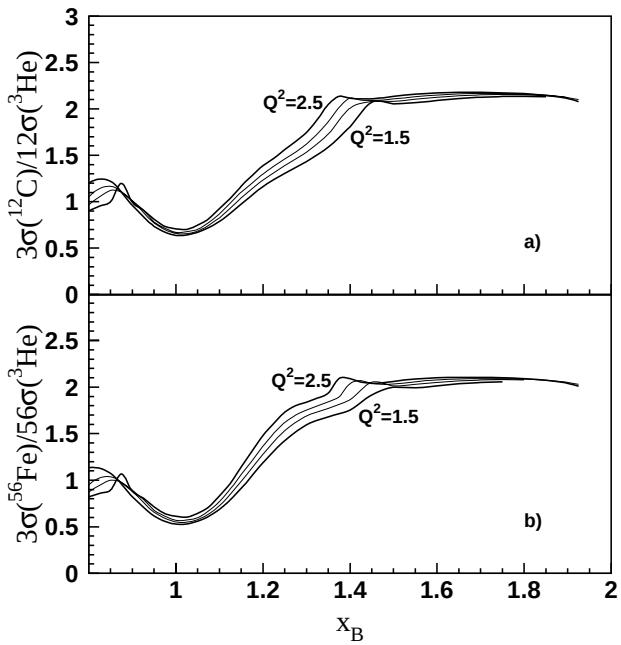

FIG. 3. SRC model predictions for the normalized inclusive cross section ratio as a function of x_B for several values of Q^2 in GeV^2. Note the scaling behavior predicted for $x_B>1.4$. (a) ^{12}C to ^{3}He, (b) ^{56}Fe to ^{3}He.

The ratios in Fig. 3 show a nice plateau starting from $x_B>1.5$ for both nuclei and all Q^2. The experimentally obtained ratio in the scaling region can be used to determine the relative probability of finding correlated NN pairs in different nuclei. However, one needs to take into account the following factors: (i) the final state interactions of a nucleon with the residual system, (ii) the NN pair center-of-mass motion, and (iii) the differences of e-p and e-n interaction cross sections (for the latter, see Sec. IV B).

In the SRC model, FSI do not destroy the scaling behavior of the ratio R. Indeed, in the light-cone approximation of the SRC model, if the invariant mass of the final NN system is sufficiently large, $\sqrt{(q+m_D)^2}-m_D>50$–100 MeV, then the scattering amplitude will depend mainly on the light-cone fraction of the interacting nucleon's momentum $\alpha=(E-p_z)/M$, and has only a weak dependence on the conjugated variables $E+p_z$ and p_t [7,20,21]. As a result, the closure approximation can be applied in the light-cone reference frame, allowing us to sum over all final states and use the fact that this sum is normalized to unity. After using the closure approximation the inclusive cross section will depend on the light-cone momentum distribution of the nucleon in the nucleus, integrated over the transverse momentum of the nucleon, $\rho_A(\alpha)$ [6]. Thus, within the light-cone description Eq. (4) measures the ratio of $\rho_A(\alpha)$ for nuclei A_1 and A_2 in the high-momentum range of the target nucleon.

In the lab frame description (in the virtual nucleon approach), however, the closure approximation cannot be applied for large values of interacting nucleon momenta, and FSI should be calculated explicitly (see, i.e., Ref. [20]). Within the SRC model at high recoil momenta, FSI are

dominated by the rescattering of the knocked-out nucleon with the correlated nucleon in the SRC [7,20]. Therefore, FSI will be localized in SRC, and will cancel in the ratio R. As a result, Eq. (4) at $x_B > x_B^0$ could be related to the ratio of high-momentum part of nucleon-momentum distributions in A_1 and A_2 nuclei [20].

Having an underlying model of the nuclear spectral functions, one can relate the measured ratios in Eq. (4) to the SRC properties of the nuclear wave function. Within the spectral function model [1], in which correlated nucleon pair is assumed at rest with the nucleon momentum distribution in pair identical to that in deuteron, the ratio in Eq. (4) could be directly related to the pernucleon SRC probability in nucleus A relative to deuterium, $a_2(A)$.

In models of the nuclear spectral function [22] in which two-nucleon correlations are moving in the mean field of the spectator $A-2$ system, the analysis of Eq. (4) will yield slightly smaller values for $a_2(A)$. Calculations by Ciofi degli Atti [23] and Simula [24] indicate that this motion does not affect the scaling but can decrease the extracted $a_2(A)$ for ^{56}Fe by up to 20%. However, it is important to emphasize that both models lead to a similar ratio of the light-cone momentum distribution for the kinematics of the present experiment.

One can summarize the predictions of the SRC model for the ratios of the inclusive cross sections from different nuclei as follows (see Fig. 3): (1) Scaling (x_B independence) is expected for $Q^2 \geqslant 1.5$ GeV^2 and $x_B^0 \leqslant x_B < 2 <$ where x_B^0 is the threshold for high recoil momentum. (2) No scaling is expected for $Q^2 < 1$ GeV^2. (3) For $x_B \leqslant x_B^0$ the ratios should have a minimum at $x_B = 1$ and should grow with x_B since heavy nuclei have a broader momentum distribution than light nuclei for $p < 0.3$ GeV/c. (4) The onset of scaling depends on Q^2; x_B^0 should decrease with increasing Q^2. (5) In the scaling regime, the ratios should be independent of Q^2. (6) In the scaling regime the ratios should depend only weakly on A for $A \geqslant 10$. This reflects nuclear saturation. (7) Ratios in the scaling region (corrected for the difference between proton and neutron form factors) are equal to the ratios of the two-nucleon SRC probabilities in the two nuclei with accuracy greater than 20%.

Another possible mechanism for inclusive (e,e') scattering at $x_B > 1$ is virtual photon absorption on a single nucleon followed by NN rescattering [25,26]. Benhar *et al.* [25] use the nuclear spectral function in the lab system and calculate the FSI using a correlated Glauber approximation (CGA), in which the initial momenta of the rescattered nucleons are neglected. In this model the cross section at $x_B > 1$ originates mainly from FSI, and therefore the cross section ratios will not scale. This model predicts that these ratios also depend on Q^2, since it includes a noticeable reduction of FSI in order to agree with the data at $Q^2 \geqslant 2$ GeV^2. Benhar *et al.* attribute this reduction in FSI to color transparency effects.[2] The requirement of large color transparency effects also results in a strong A dependence of the ratio since the amount of the FSI suppression depends on the number of nucleons participating in the rescattering.

The main predictions of the CGA model for the nuclear cross section ratios are as follows: (1) No scaling is predicted at $Q^2 \geqslant 1$ GeV^2 and $x_B < 2$. (2) The nuclear ratios should vary with Q^2. (3) The ratios should depend on A. (4) The model is not applicable at $Q^2 < 1$ GeV^2.

Thus, measuring the ratios of inclusive (e,e') scattering at $x_B > 1$ and $Q^2 > 1$ GeV^2 will yield important information about the reaction dynamics. If scaling is observed, then the dominance of the SRC in the nuclear wave function is manifested and the measured ratios will contain information about the probability of two-nucleon short range correlations in nuclei.

III. EXPERIMENT

In this paper we present the first experimental studies of ratios of normalized and acceptance- and radiative-corrected inclusive yields of electrons scattered from ^{4}He, ^{12}C, ^{56}Fe, and ^{3}He measured under identical kinematical conditions.

The measurements were performed with the CEBAF large acceptance spectrometer (CLAS) in Hall B at the Thomas Jefferson National Accelerator Facility. This is the first CLAS experiment with nuclear targets. Electrons with 2.261 and 4.461 GeV energies incident on ^{3}He, ^{4}He, ^{12}C, and ^{56}Fe targets have been used. We used helium liquefied in cylindrical target cells 1 cm in diameter and 4 cm long, positioned on the beam approximately in the center of the CLAS. The solid targets were thin foils of ^{12}C (1 mm) and ^{56}Fe (0.15 mm) positioned 1.5 cm downstream of the exit window of the liquid target. Data on solid targets have been taken with an empty cell of liquid targets. The CLAS vertex position resolution is better than 2.2 mm (σ), allowing us to completly cut out the target cell contribution in the solid target data. In the case of liquid targets (^{3}He and ^{4}He) we make 3-cm vertex cuts in the central part of cells. The estimated contribution from the two 15 μm target cell windows is less than 0.1%.

The CLAS detector [28] consists of six sectors, each functioning as an independent magnetic spectrometer. Six superconducting coils generate a toroidal magnetic field primarily in the azimuthal direction. Each sector is instrumented with multiwire drift chambers [29] and time-of-flight scintillator counters [30] that cover the angular range from 8° to 143°, and, in the forward region ($8° < \theta < 45°$), with gas-filled threshold Cherenkov counters (CC) [31] and lead-scintillator sandwich-type electromagnetic calorimeters (EC) [32]. Azimuthal coverage for CLAS is limited only by the magnetic coils, and is approximately 90% at large polar angles and 50% at forward angles. The CLAS was triggered on scattered electrons by a CC-EC coincidence at 2.2-GeV and by the EC alone with a ≈ 1 GeV electron threshold at 4.4 GeV.

For our analysis, electrons are selected in the kinematical region $Q^2 > 0.65$ GeV^2 and $x_B > 1$ where the contribution from the high-momentum components of the nuclear wave function should be enhanced.

We also require that the energy transfer ν should be

[2]So far, no color transparency effects are observed in $A(e,e'p)X$ reactions at $Q^2 \leqslant 8$ GeV^2 [27].

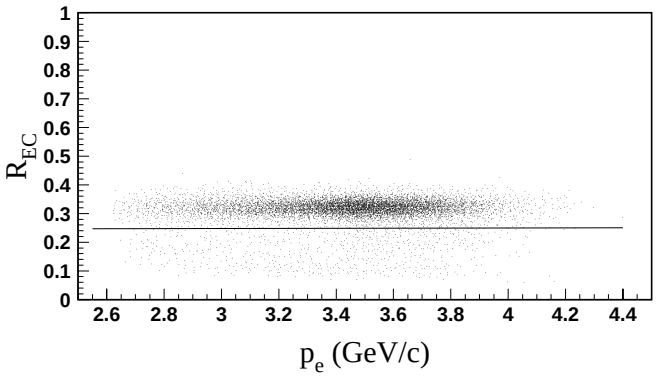

FIG. 4. The ratio R_{EC} of energy deposited in the CLAS electromagnetic calorimeter (EC) to the electron momentum p_e as a function of p_e at beam energy 4.461 GeV. The line at $R_{EC}\approx 0.25$ is located three standard deviations below the mean, as determined by measurements at several values of p_e. This cut was used to identify electrons.

$>$300 MeV (the characteristic missing energy for SRC is $\sim$260 MeV [1]). In this region one expects that inclusive $A(e,e')$ scattering will proceed through the interaction of the incoming electron with a correlated nucleon in a SRC.

A. Electron identification

Electrons were selected in the fiducial region of the CLAS sectors. The fiducial region is a region of azimuthal angle, for a given momentum and polar angle, where the electron detection efficiency is constant. Then a cut on the ratio of the energy deposited in the EC to the measured electron momentum p_e (R_{EC}) was used for final selection. In Fig. 4, R_{EC} vs p_e for the ^{56}Fe target at 4.4 GeV is shown. The line shows the applied cut at $R_{EC}\approx 0.25$, which is located three standard deviations below the mean as determined by measurements at several values of p_e. A Monte Carlo simulation showed that these cuts reduce the $A(e,e')$ yield by less than 0.5%.

We estimated the π^- contamination in the electron sample for a wide angular range using the photoelectron distributions in the CLAS Cherenkov counters. We found that this is negligible for $x_B>1$.

B. Acceptance corrections

We used the Monte Carlo techniques to determine the electron acceptance correction factors. Two iterations were done to optimize the cross section model for this purpose. In the first iteration we generated events using the SRC model [12] and determined the CLAS detector response using the GEANT-based CLAS simulation program, taking into account "bad" or "dead" hardware channels in various components of CLAS, as well as realistic position resolution for the CLAS drift chambers. We then used the CLAS data analysis package to reconstruct these events using the same electron identification criterion that was applied to the real data. The acceptance correction factors were found as the ratios of the number of reconstructed and simulated events in each kinematic bin. Then the acceptance corrections were applied to the data event by event, i.e., each event was weighted by the acceptance factor obtained for the corresponding $(\Delta x_B,\Delta Q^2)$ kinematic bin, and the cross sections were calculated as a function of x_B and Q^2. For the second iteration the obtained cross sections were fitted and the fit functions were used to generate a new set of data, and the process was repeated. Figure 5 shows the electron acceptance factors after the second iteration for liquid (^{3}He) and solid (^{12}C) targets. We used the difference between the iterations as the uncertainty in the acceptance correction factor. Note that the acceptance for the carbon target is smaller than that for the helium target. This is due to the closer location of the solid targets to the CLAS coils, which limits azimuthal angular coverage of the detectors.

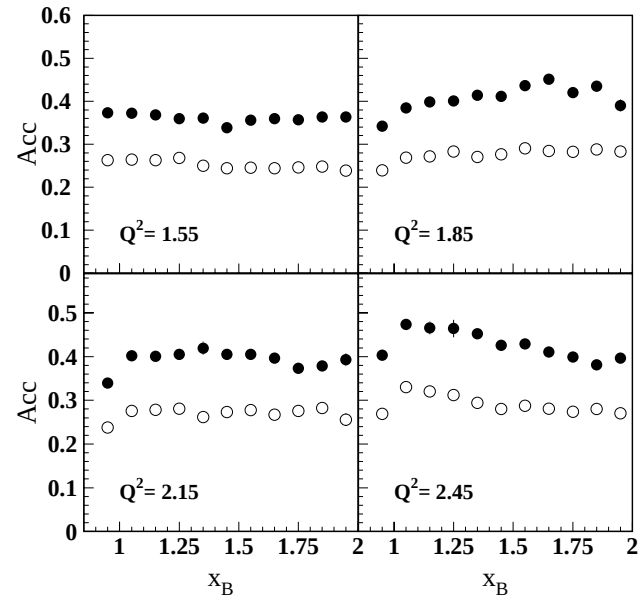

FIG. 5. The acceptance correction factors as a function of x_B. ● is for ^{3}He and ○ for ^{12}C. Q^2 are in GeV^2.

C. Radiative corrections

The cross section ratios were corrected for radiative effects. The radiative correction for each target as a function of Q^2 and x_B was calculated as the ratio

$$C_{rad}(x_B,Q^2)=\frac{d\sigma^{rad}(x_B,Q^2)}{d\sigma^{norad}(x_B,Q^2)}, \tag{5}$$

where $d\sigma^{rad}(x_B,Q^2)$ and $d\sigma^{norad}(x_B,Q^2)$ are the radiatively corrected and uncorrected theoretical cross sections, respectively. The cross sections have been calculated using Ref. [33] which is based on the adaptation of the formalism of Ref. [34] for inclusive and semi-inclusive (e,e') reactions on nuclear targets.

IV. RESULTS

We constructed ratios of normalized, and acceptance- and radiative-corrected inclusive electron yields on nuclei ^{4}He, ^{12}C, and ^{56}Fe divided by the yield of ^{3}He in the range of

kinematics $1<x_B<2$. Assuming that electron detection efficiency from different targets is the same, these ratios, weighted by atomic number, are equivalent to the ratios of cross sections in Eq. (4).

The normalized yields for each x_B and Q^2 bin have been calculated as

$$\frac{d\mathcal{Y}}{dQ^2dx_B}=\frac{N_{e'}}{\Delta Q^2\Delta x_B N_e N_T}\frac{1}{\mathrm{Acc}}, \tag{6}$$

where N_e and N_T are the number of incident electrons and target nuclei, respectively, Acc is the acceptance correction factor, and ΔQ^2 and Δx_B are the bin sizes in Q^2 and in x_B, respectively. Since electron detection efficiency in CLAS is expected to be $>96\%$, we compare the obtained yields with radiated cross sections calculated by Ref. [12] code. Within systematic uncertainties (see below), satisfactory agreement has been found between our results and the calculations from Ref. [12], which were tuned on SLAC date [17] and described reasonably well [18] at the Jefferson Lab Hall C [19] data.

The ratios $R(A,{}^3\mathrm{He})$, also corrected for radiative effects, are defined as

$$R(A,{}^3\mathrm{He})=\frac{3\mathcal{Y}(A)}{A\mathcal{Y}({}^3\mathrm{He})}\frac{C^A_{Rad}}{C^{{}^3\mathrm{He}}_{Rad}}, \tag{7}$$

where $\mathcal{Y}$ is the normalized yield in a given (Q^2,x_B) bin and C^A_{Rad} is the radiative correction factor from Eq. (5) for each nucleus. The ratio of the radiative correction factors in Eq. (7) is independent of x_B at $x_B>1$, and is ≈ 0.95 and 0.92 for ^{12}C and ^{56}Fe, respectively.

Figure 6 shows these ratios for ^{12}C at several values of Q^2. Figures 7 and 8 show these ratios for ^{4}He and ^{56}Fe, respectively. These data have the following important characteristics.

(a) There is a clear Q^2 evolution of the shape of ratios. At low Q^2 ($Q^2<1.4$ GeV^2), $R(A,{}^3\mathrm{He})$ increases with x_B in the entire $1<x_B<2$ range [see Figs. 6(a), 7(a), and 8(a)]. At high Q^2 ($Q^2\geqslant 1.4$ GeV^2), $R(A,{}^3\mathrm{He})$ is independent of x_B for $x_B>x_B^0\approx 1.5$ [see Figs. 6(b), 7(b), and 8(b)]. (b) The value of $R(A,{}^3\mathrm{He})$ in the scaling regime is independent of Q^2. (c) The value of $R(A,{}^3\mathrm{He})$ in the scaling regime for $A>10$ suggests a weak dependence on target mass.

A. Systematic errors

The systematic errors in this measurement are different for different targets and include uncertainties in (a) fiducial cut applied: $\approx 1\%$, (b) radiative correction factors: $\approx 2\%$, (c) target densities and thicknesses: $\approx 0.5\%$ and 1.0% for solid targets, and 0.5% and 3.5% for liquid targets, respectively. (d) acceptance correction factors (Q^2 dependent): between 2.2% and 4.0% for solid targets and between 1.8% and 4.3% for liquid targets.

Some of systematic uncertainties will cancel out in the yield ratios. For the ^{4}He/^{3}He ratio, all uncertainties except those on the beam current and the target density divide out, giving a total systematic uncertainty of 0.7%.

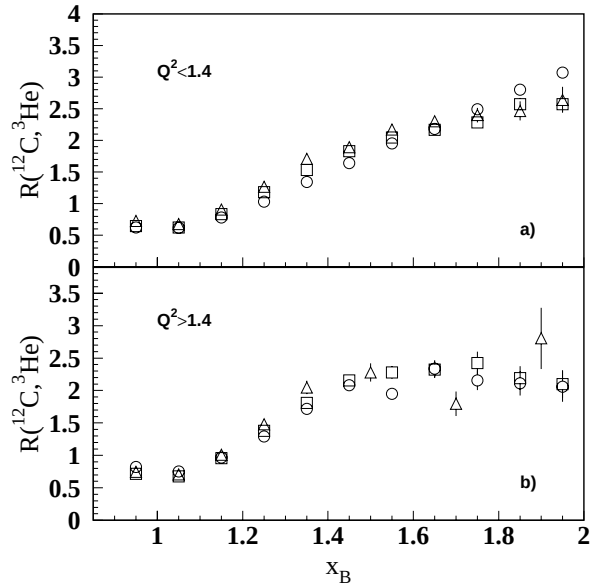

FIG. 6. $R({}^{12}\mathrm{C},{}^3\mathrm{He})$, the pernucleon yield ratios for ^{12}C to ^{3}He. (a) ○ is for $0.65<Q^2<0.85$, □ for $0.9<Q^2<1.1$, and △ for $1.15<Q^2<1.35$ GeV^2, all at incident energy 2.261 GeV. (b) ○ is for $1.4<Q^2<1.6$ GeV^2 at incident energy 2.261 GeV, □ for $1.4<Q^2<2.0$, and △ $2.0<Q^2<2.6$ GeV^2, both at incident energy 4.461 GeV. Statistical errors are shown only.

For the solid target to ^{3}He ratios, only the electron detection efficiency cancels. The quadratic sum of the other uncertainties is between 5% and 7%, depending on Q^2. The systematic uncertainties on the ratios for all targets and Q^2 are presented in Table I. Note that, since the cross sections are rapidly varying with x_B, the weighted centroid of each bin is not at the center of the bin. However, since in the scaling region the cross section ratios are constant, this effect cancels.

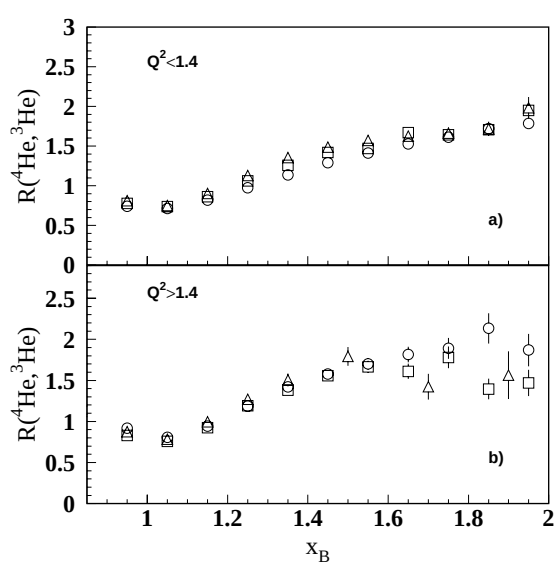

FIG. 7. The same as Fig. 6, but for ^{4}He.

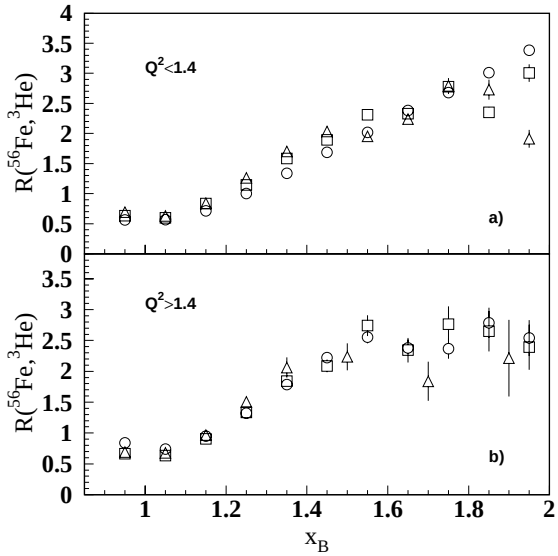

FIG. 8. The same as Fig. 6, but for ^{56}Fe.

B. Probabilities of two-nucleon short range correlations in nuclei

Our data are clearly consistent with the predictions of the *NN* SRC model. The obtained ratios $R(A,{}^3\mathrm{He})$ for $1.4<Q^2<2.6$ GeV^2 region are shown in Table II as a function of x_B. Figure 9 shows these ratios for the ^{12}C and ^{56}Fe targets together with the SRC calculation results using Ref. [12], which used the estimated scaling factors $a_2(A)$ (per-nucleon probabilitiy of *NN* SRC in nucleus *A*) from Ref. [7]. Good agreement between our data and calculation is seen. Note that one of the goals of the present paper is to determine these factors more precisely (see below).

Experimental data in the scaling region can be used to estimate the relative probabilities of *NN* SRC in nuclei compared to ^{3}He. According to Ref. [1] the ratio of these probabilities is proportional to

$$r(A,{}^3\mathrm{He})=\frac{(2\sigma_p+\sigma_n)\sigma(A)}{(Z\sigma_p+N\sigma_n)\sigma({}^3\mathrm{He})}, \tag{8}$$

where $\sigma(A)$ and $\sigma({}^3\mathrm{He})$ are the $A(e,e')$ and $^3\mathrm{He}(e,e')$ inclusive cross sections, respectively. σ_p and σ_n are the electron-proton and electron-neutron elastic scattering cross sections respectively. *Z* and *N* are the number of protons and neutrons in nucleus *A*. Using Eq. (4) the ratio of Eq. (8) can be related to the experimentally measured ratios $R(A,{}^3\mathrm{He})$ as

TABLE I. Systematic uncertainties $\delta R(A)$, $\delta R({}^4\mathrm{He})$ for the ratios of normalized inclusive yields, $R(A,{}^3\mathrm{He})$ ($A={}^{12}\mathrm{C},{}^{56}\mathrm{Fe}$) and $R({}^4\mathrm{He},{}^3\mathrm{He})$. $\Delta Q^2=\pm 0.15$ GeV^2.

Q^2 (GeV)^2	1.55	1.85	2.15	2.45
$\delta R(A)$	7.1	5.8	4.9	5.1
$\delta R({}^4\mathrm{He})$	0.7	0.7	0.7	0.7

TABLE II. The ratios $R(A,{}^3\mathrm{He})$, measured in $1.4<Q^2<2.6$ GeV^2 interval. Errors are statistical only.

X_B	^{4}He	^{12}C	^{56}Fe
0.95±0.05	0.86±0.004	0.77±0.003	0.80±0.004
1.05±0.05	0.78±0.004	0.72±0.003	0.72±0.004
1.15±0.05	0.94±0.006	0.96±0.006	0.94±0.007
1.25±0.05	1.19±0.012	1.33±0.012	1.33±0.015
1.35±0.05	1.41±0.021	1.77±0.025	1.81±0.030
1.45±0.05	1.58±0.033	2.12±0.044	2.17±0.055
1.55±0.05	1.71±0.049	2.12±0.059	2.64±0.087
1.65±0.05	1.70±0.063	2.29±0.085	2.40±0.109
1.75±0.05	1.85±0.089	2.32±0.110	2.45±0.139
1.85±0.05	1.65±0.100	2.21±0.128	2.70±0.190
1.95±0.05	1.71±0.124	2.17±0.157	2.57±0.227

$$r(A,{}^3\mathrm{He})=R(A,{}^3\mathrm{He})\times\frac{A(2\sigma_p+\sigma_n)}{3(Z\sigma_p+N\sigma_n)}. \tag{9}$$

To obtain the numerical values for $r(R,{}^3\mathrm{He})$, we calculated the second factor in Eq. (9) using parametrizations for the neutron and proton form factors [35]. We found the average values of these factors to be 1.14 ± 0.02 for ^{4}He and ^{12}C, and 1.18 ± 0.02 for ^{56}Fe. Note that these factors vary slowly over our Q^2 range. For $r(A,{}^3\mathrm{He})$ calculations, the experimental data were integrated over $Q^2>1.4$ GeV^2 and $x_B>1.5$ for each nucleus. The ratio of integrated yields, $R(A,{}^3\mathrm{He})$, is presented in the first row of Table III and in Fig. 10(a) (open circles). The ratios $r(A,{}^3\mathrm{He})$ are shown in the second row of Table III and by the filled circles in Fig. 10(a). One can see that the ratios $r(A,{}^3\mathrm{He})$ are 2.5–3.0 for ^{12}C and ^{56}Fe, and approximately 1.95 for ^{4}He.

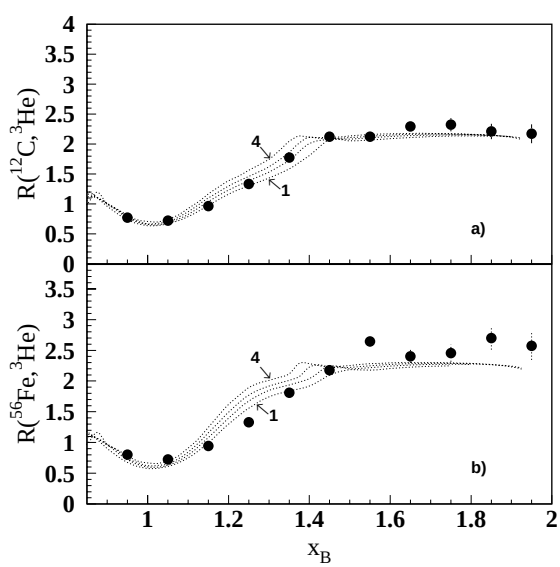

FIG. 9. $R(A,{}^3\mathrm{He})$ as a function of x_B for $1.4<Q^2<2.6$ GeV^2, statistical errors are shown only. Curves are SRC model predictions for different Q^2 in the range 1.4 GeV^2 (curve 1) to 2.6 GeV^2 (curve 4), respectively, for (a) ^{12}C, (b) ^{56}Fe.

TABLE III. $R(A,{}^3\mathrm{He})$ and $r(A,{}^3\mathrm{He})$ are the ratios of normalized (e,e') yields for nucleus A to ^{3}He, and the relative per nucleon probabilities of SRC for the two nuclei. $a_2(A)^{Expt.}$ and $a_2(A)^{theor}$ are the $a_2(A)$ parameters obtained by multiplying $r(A,{}^3\mathrm{He})$ with the experimental and/or theoretical values of $a_2(3)$. The statistical (first) and systematic (second) errors are shown. In statistical errors for $a_2(A)^{Expt.}$ and $a_2(A)^{theor}$, the uncertainties of $a_2(3)$ are included. Systematic errors for ^{12}C and ^{56}Fe are calculated using the acceptance uncertainties averaged over entire Q^2 range (see Table I). Note that there is a theoretical uncertainty converting $R(A,{}^3\mathrm{He})$ ratios into SRC probabilities, which is maximum for ^{56}Fe and is no more than 20% [23]. $a_2(A)^{aver}$ is an average (weighted) of $a_2(A)^{Expt.}$ and $a_2(A)^{theor}$. To obtain the systematic errors of $a_2(A)^{aver}$, the systematic uncertainties of $a_2(A)^{Expt.}$ and $a_2(A)^{theor}$ were added in quadrature.

	^{4}He	^{12}C	^{56}Fe
$R(A,{}^3\mathrm{He})$	$1.72\pm0.03\pm0.012$	$2.20\pm0.04\pm0.12$	$2.54\pm0.06\pm0.14$
$r(A,{}^3\mathrm{He})$	$1.96\pm0.05\pm0.014$	$2.51\pm0.06\pm0.14$	$3.00\pm0.08\pm0.17$
$a_2(A)^{Expt.}$	$3.33\pm0.59\pm0.023$	$4.27\pm0.76\pm0.24$	$5.11\pm0.91\pm0.29$
$a_2(A)^{theor}$	$3.92\pm0.22\pm0.027$	$5.02\pm0.28\pm0.29$	$6.00\pm0.34\pm0.34$
$a_2(A)^{aver}$	$3.85\pm0.21\pm0.027$	$4.93\pm0.27\pm0.28$	$5.90\pm0.32\pm0.34$

The pernucleon SRC probability in nucleus A relative to ^{3}He is proportional to $r(A,{}^3\mathrm{He})\sim a_2(A)/a_2(3)$, where $a_2(A)$ and $a_2(3)$ are the pernucleon probabilities of SRC relative to deuterium for nucleus A and ^{3}He. As was discussed earlier, the direct relation of $r(A,{}^3\mathrm{He})$ to the pernucleon probabilities of SRC has an uncertainty of up to 20% due to pair center-of-mass motion. Within this uncertainty, we will define the pernucleon SRC probabilities of nuclei relative to deuterium as

$$a_2(A)=r^A_{{}^3\mathrm{He}}\cdot a_2(3). \tag{10}$$

Two values of $a_2(3)$ have been used to calculate $a_2(A)$. First is the experimentally obtained value from Ref. [7], $a_2(3)=1.7\pm0.3$, and the second is the value from the calculation using the wave function for deuterium and ^{3}He, $a_2(3)=2\pm0.1$. Similar results were obtained in Ref. [36].

The pernucleon probability of SRC for nucleus A relative to deuterium is shown in the third and fourth rows of Table III and in Fig. 10(b) where the results from Ref. [7] are shown as well.

In fifth row of the Table III, averages of $a_2(A)^{Expt.}$ and $a_2(A)^{theor}$ are shown. One can see that $a_2(A)$ changes rapidly from $A=4$ to $A=12$, while for $A\geqslant12$ it changes very slowly. There are approximately 4.9–5.9 times as much SRC for $A\geqslant12$ than for deuterium, and approximately 3.8 times as much SRC for ^{4}He as for deuterium. These results are consistent with the analysis of the previous SLAC (e,e') data [7]. They are also consistent with calculations of Ref. [36]. Figure 11 shows the measured Q^2 dependence of the relative SRC probability, $a_2(A)$, which appears to be Q^2 independent for all targets.

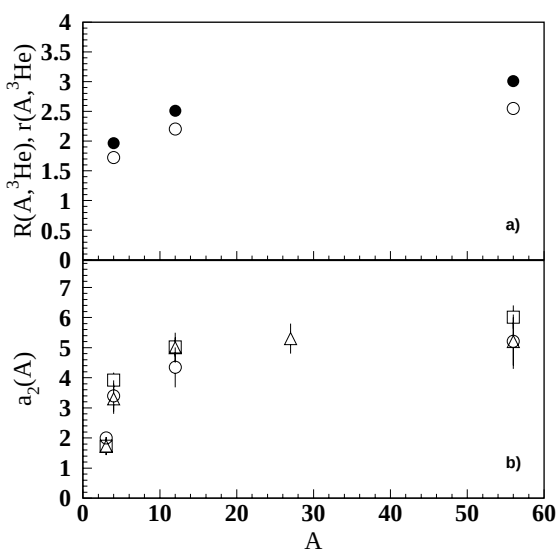

FIG. 10. (a) $R(A,{}^3\mathrm{He})$ (○) and $r(A,{}^3\mathrm{He})$ (●) versus A. (b) $a_2(A)$ versus A. ○—$a_2(A)$ obtained from Eq. (10) using the experimental value of $a_2(3)$ from Ref. [7]; □—$a_2(A)$ obtained using the theoretical value of $a_2(3)$. △—data from Ref. [7]. For errors shown, see caption of Table III.

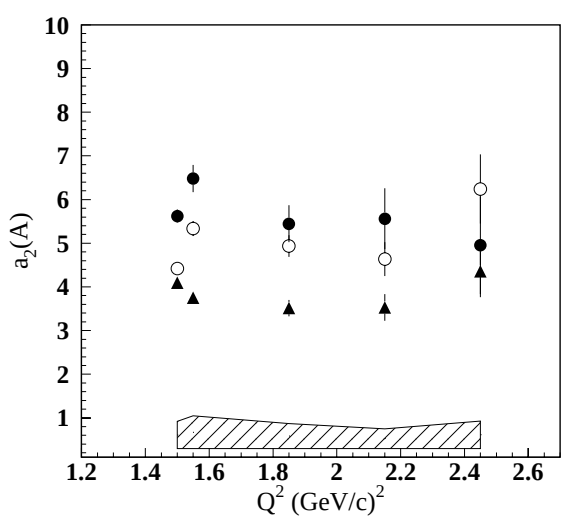

FIG. 11. Q^2 dependences of $a_2(A)$ parameters obtained by multiplying $r(A,{}^3\mathrm{He})$ with the theoretical values of $a_2(3)$. Error bars are statistical only (see caption of Table III). Shadowed area shows systematic error band. Q^2 bin sizes are ±0.15 GeV^2. ● is for ^{56}Fe, ○ for ^{12}C, and ▲ for ^{4}He.

V. SUMMARY

The $A(e,e')$ inclusive electron scattering cross section ratios of ^{4}He, ^{12}C, and ^{56}Fe to ^{3}He have been measured for the first time under identical kinematical conditions. The following are shown.

(1) These ratios are independent of x_B (scale) for $x_B > 1.5$ and $Q^2 > 1.4$ GeV^2, i.e., for high recoil momentum. The ratios do not scale for $Q^2 < 1.4$ GeV^2.

(2) These ratios in the scaling region are independent of Q^2, and change very slowly in $A \geqslant 12$ range.

(3) These features were predicted by the short range correlation model and consistent with the kinematical expectation that two-nucleon short range correlations are dominating in the nuclear wave function at $p_m \gtrsim 300$ MeV/c.

(4) The observed scaling shows that momentum distributions at high momenta have the same shape for all nuclei and differ only by a scale factor.

(5) Using the SRC model, combined with the (measured and/or calculated) ^{3}He/D ratio, the values of ratios in the scaling region were used to derive the relative probabilities of SRC in nuclei compared to deuterium. The pernucleon probability of short range correlations in nuclei relative to deuterium is ≈ 3.8 times larger for ^{4}He and approximately 4.9 and 5.9 times larger for ^{12}C and ^{56}Fe.

ACKNOWLEDGMENTS

We acknowledge the efforts of the staff of the Accelerator and Physics Divisions (especially the Hall B target group) at the Jefferson Lab in their support of this experiment. We also acknowledge useful discussions with D. Day and E. Piasetzki. This work was supported in part by the U.S. Department of Energy, the National Science Foundation, the French Commissariat a l'Energie Atomique, the French Center National de la Recherche Scientifique, the Italian Istituto Nazionale di Fisica Nucleare, and the Korea Research Foundation. U.T. acknowledges an ''Emmy Noether'' grant from the Deutsche Forschungsgemeinschaft. The Southeastern Universities Research Association (SURA) operates the Thomas Jefferson National Accelerator Facility for the United States Department of Energy under Contract No. DE-AC05-84ER40150.

[1] L.L. Frankfurt and M.I. Strikman, Phys. Rep. **76**, 215 (1981); **160**, 235 (1988).
[2] T.W. Donnelly and I. Sick, Phys. Rev. C **60**, 065502 (1999).
[3] J. Arrington *et al.*, Phys. Rev. Lett. **82**, 2056 (1999).
[4] S.C. Pieper, R.B. Wiringa, and V.R. Pandharipande, Phys. Rev. C **46**, 1741 (1992).
[5] C. Ciofi degli Atti and S. Simula, Phys. Rev. C **53**, 1689 (1996).
[6] L. Frankfurt and M. Strikman, in *Electromagnetic Interactions with Nuclei*, edited by B. Frois and I. Sick (World Scientific, Singapore, 1991).
[7] L.L. Frankfurt, M.I. Strikman, D.B. Day, and M.M. Sargsyan, Phys. Rev. C **48**, 2451 (1993).
[8] W.P. Schutz *et al.*, Phys. Rev. Lett. **38**, 8259 (1977).
[9] S. Rock *et al.*, Phys. Rev. Lett. **49**, 1139 (1982).
[10] R.G. Arnold *et al.*, Phys. Rev. Lett. **61**, 806 (1988).
[11] D. Day *et al.*, Phys. Rev. Lett. **59**, 427 (1979).
[12] M. Sargsian, Report No. CLAS-NOTE 90-007, 1990 (unpublished).
[13] M.M. Sargsian, Ph.D. thesis, Yerevan, 1993.
[14] R. Machleidt, Phys. Rev. C **63**, 024001 (2001).
[15] M.V. Zverev and E.E. Saperstein, Yad. Fiz. **43**, 304 (1986).
[16] A. Bodek *et al.*, Phys. Rev. D **20**, 1471 (1979).
[17] D. Day *et al.*, Phys. Rev. Lett. **43**, 1143 (1979).
[18] M.M. Sargsian (unpublished).
[19] Th. C. Petitjean, Inaugural-Dissertation, Basel, 2000 (unpublished).
[20] L.L. Frankfurt, M.M. Sargsian, and M.I. Strikman, Phys. Rev. C **56**, 1124 (1997).
[21] M. Sargsian, Int. J. Mod. Phys. E **10**, 405 (2001).
[22] C. Ciofi degli Atti, S. Simula, L.L. Frankfurt, and M.I. Strikman, Phys. Rev. C **44**, 7 (1991).
[23] C. Ciofi degli Atti (private communication).
[24] S. Simula, in *Proceedings of the PANIC XIII, Perugia, Italy, 1993*, edited by A. Pascolini (World Scientific, Singapore, 1994), p. 448.
[25] O. Benhar *et al.*, Phys. Rev. C **44**, 2328 (1991).
[26] O. Benhar *et al.*, Phys. Lett. B **343**, 47 (1995).
[27] K. Garrow *et al.*, Phys. Rev. C **66**, 044613 (2002).
[28] B.A. Mecking *et al.*, Nucl. Instrum. Methods Phys. Res. A **505**, 513 (2003); W. Brooks, Nucl. Phys. **A663**, 1077c (2000).
[29] M.D. Mestayer *et al.*, Nucl. Instrum. Methods Phys. Res. A **449**, 81 (2000).
[30] E.S. Smith *et al.*, Nucl. Instrum. Methods Phys. Res. A **432**, 265 (1999).
[31] G. Adams *et al.*, Nucl. Instrum. Methods Phys. Res. A **465**, 414 (2001).
[32] M. Amarian *et al.*, Nucl. Instrum. Methods Phys. Res. A **460**, 239 (2001).
[33] M. M. Sargsian, Report No. YERPHI-1331-26-91 1991 (unpublished).
[34] L.W. Mo and Y.S. Tsai, Rev. Mod. Phys. **41**, 205 (1969).
[35] P.E. Bosted *et al.*, Phys. Rev. C **51**, 409 (1995).
[36] J.L. Forest *et al.*, Phys. Rev. C **54**, 646 (1996).